



Auditory Temporal Computation: Interval Selectivity Based on Post-Inhibitory Rebound

EDWARD W. LARGE

*Center for Complex Systems and Brain Sciences, Florida Atlantic University, 777 Glades Road,
P.O. Box 3091, Boca Raton, FL 33431-0991, USA*

large@walt.ccs.fau.edu

JOHN D. CRAWFORD

*Graduate Group in Neuroscience & Psychology Department, University of Pennsylvania,
3815 Walnut St. Philadelphia, PA 19104, USA*

crawford@psych.upenn.edu

Received October 26, 2001; Revised May 15, 2002; Accepted May 22, 2002

Action Editor: John P. Miller

Abstract. The measurement of time is fundamental to the perception of complex, temporally structured acoustic signals such as speech and music, yet the mechanisms of temporal sensitivity in the auditory system remain largely unknown. Recently, temporal feature detectors have been discovered in several vertebrate auditory systems. For example, midbrain neurons in the fish *Pollimyrus* are activated by specific rhythms contained in the simple sounds they use for communication. This poses the significant challenge of uncovering the neuro-computational mechanisms that underlie temporal feature detection. Here we describe a model network that responds selectively to temporal features of communication sounds, yielding temporal selectivity in output neurons that matches the selectivity functions found in the auditory system of *Pollimyrus*. The output of the network depends upon the timing of excitatory and inhibitory input and post-inhibitory rebound excitation. Interval tuning is achieved in a behaviorally relevant range (10 to 40 ms) using a biologically constrained model, providing a simple mechanism that is suitable for the neural extraction of the relatively long duration temporal cues (i.e. tens to hundreds of ms) that are important in animal communication and human speech.

Keywords: auditory perception, temporal processing, communication, oscillation, post-inhibitory rebound

Introduction

The timing of sensory stimuli carries information critical to a wide range of behaviors. Temporal patterns are important for visual object recognition in humans (Lee and Blake, 1999) and for visual species recognition in a variety of animals (Salmon and Atsides, 1968; Jenssen, 1970; Lloyd, 1975). Similarly, the temporal structure of sounds is essential for auditory stream segregation (Bregman, 1990), music perception (Large

and Jones, 1999), and animal communication (Hoy et al., 1982; Huber and Thorson, 1985; Gerhardt, 1994; Myrberg, 1997). Despite the widespread importance of temporal analysis in behavior, relatively little is known about the fundamental neuro-computational mechanisms that underlie the extraction of temporal information. In this paper we develop a computational model of a brain mechanism for temporal feature extraction.

Neurons that respond selectively to temporal features of communication sounds have been discovered

in the central auditory systems of a variety of animal species (Rose and Capranica, 1985; Plassmann, 1985; Langner and Schreiner, 1988; Feng et al., 1990; Diekamp and Gerhardt, 1995; Crawford, 1997; Penna et al., 1997; Bodnar and Bass, 1999). In these examples, action potentials produced by primary afferent neurons are temporally synchronized to the low frequency sounds often used in communication, and thus provide a temporal representation of sounds to higher-order circuits. Trains of action potentials generated in the auditory nerve may then be used to compute a rate-place code in higher auditory areas. The computational mechanisms that transform peripheral trains of action potentials into feature selective auditory responses, however, are only beginning to be understood (Langner, 1992; Hooper, 1998; Alder and Rose, 1998, 2000; Fortune and Rose, 2000; Casseday et al., 2000).

The African fish *Pollimyrus* has been developed as a model system for studying auditory temporal computation. These fish use simple low frequency sounds for courtship communication (Fig. 1) and have gas-filled bladders in their ears for detecting sound pressure (Fletcher and Crawford, 2001). Like other fishes, they lack an elaborate peripheral structure for frequency analysis (e.g., the mammalian cochlea), and do not exhibit the degree of mechanical frequency decomposition that is seen in other vertebrates (Popper and Coombs, 1982). Thus temporal analysis of sounds appears to be particularly important in fishes.

Male *Pollimyrus* produce grunts and moans in alternation while interacting with females on their territories (Crawford, 1997; Crawford and Huang, 1999). Grunts

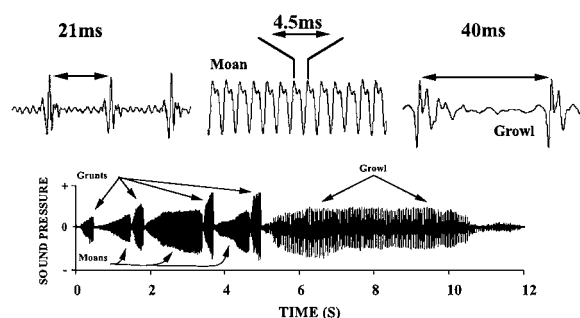


Figure 1. Natural communication sounds produced by a male *Pollimyrus adspersus*. An entire acoustic display, recorded with a hydrophone, is shown (below), and expanded waveform segments are shown (above) for each of the three constituent sounds, illustrating the fine structure and differences in inter-click interval (ICI). Adapted from Crawford (1997), with permission.

are acoustic click trains (click duration ≈ 5 ms) with an inter-click-interval (ICI) of about 18 ms and duration of 250 ms. Moans are continuous, near-sinusoidal, sounds with a period of about 4 ms and duration of 800 ms. The sounds made by closely related *Pollimyrus* species (*P. adspersus* and *P. isidori*) are clearly distinguished by differences in the fundamental period of these sounds and individual males are so stereotyped in their production that the sounds also serve as individual signatures among conspecific males (Crawford et al., 1997). The fish readily discriminate small differences between the sounds of different species and different individuals (Marvit and Crawford, 2000). One of the major functions of the *Pollimyrus* auditory system is the analysis of these simple courtship sounds.

Neurophysiological studies of *Pollimyrus* indicate that an initial temporal representation of sound, created in the ear and auditory nerve, is used by central brain circuits to compute specific temporal features thus creating a *rate-place code* for time intervals. Responses to tones in the auditory nerve of *Pollimyrus* consist of trains of spikes, sustained for the duration of the tone, and the inter-spike intervals correspond exactly to the stimulus period ($\pm 20 \mu s$) with a single spike corresponding to every stimulus cycle (Kozloski and Crawford, 1997, 1998a; Suzuki and Crawford, 2000; Suzuki et al., submitted). Responses to grunt-like click trains are similar, with spikes synchronized to the individual clicks. These responses are largely independent of the period of the stimulus used. In contrast, the synchronization of midbrain neurons is less precise and some neurons show strong response-dependence on stimulus period. Interval selective neurons are activated best over a narrow range of inter-click intervals when stimulated with click trains, seen by plotting action potential rate as a function of ICI (interval-selectivity curves; Crawford, 1997). These *feature selective neurons* represent a significant transformation of the input to this area of the brain and our focus here is on the computational mechanism that yields these transformations.

We have hypothesized that the selectivity of midbrain neurons emerges through a network computation that depends upon a simple set of synaptic connections and well known intrinsic properties of neurons (Crawford, 1997; Cudmore et al., 1998). Specifically, synaptic inhibition and subsequent rebound depolarization (*inhibitory rebound*) can form the basis of a temporal gate, with the duration of inhibition determining the temporal position of a window during which

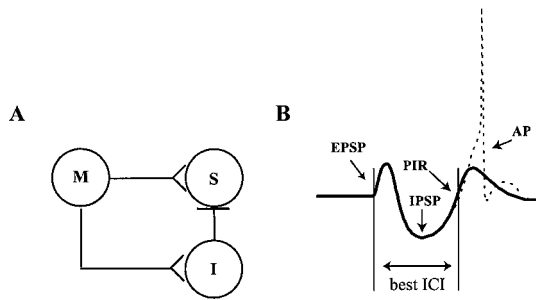


Figure 2. A model of interval selectivity based on post-inhibitory rebound. **A:** A schematic model of the interval selective circuit. Neuron **M** projects from the medulla, branches, and excites neurons **I** and **S** in the mesencephalon. Neuron **I** is an inhibitory interneuron whose input to **S** is slightly delayed by the **M** to **I** synapse. **B:** The intracellular events that might be recorded from the interval selective neuron **S** during auditory stimulation. A single click yields an excitatory post synaptic potential (EPSP) and an inhibitory post synaptic potential (IPSP) followed by rebound excitation (PIR), but no action potential. However a second click, appropriately timed, will coincide temporally with post inhibitory rebound, generating an action potential. With click trains as input, the circuit shown in **A** is *interval selective*, having a preferred interval at which the probability of firing action potentials reaches a maximum.

inputs are facilitated (Edwards, 1983; Sullivan, 1982; Margoliash, 1983; Casseday et al., 1994). In order for this mechanism to generate interval selectivity for click trains in *Pollimyrus*, selective neurons must receive excitatory input from neurons that deliver synchronized spike trains, receive inhibitory input that is similarly synchronized and which yields long lasting inhibition and produces rebound depolarization (Fig. 2A).

In this paper we investigate the inhibitory gating hypothesis by developing a relatively simple, biophysically constrained network model, and making quantitative comparisons of its response properties to those of real interval-selective neurons studied in the mid-brain of *Pollimyrus*. We investigate the properties of the proposed mechanism through mathematical modeling. The biophysical properties used in the model are derived from voltage clamp studies of neurons in a variety of animals, but are assumed to exist also in *Pollimyrus*. We begin by developing an initial model based purely on inhibitory gating, and we compare its behavior to that of real neurons. Based on this analysis we augment the model, adding synaptic depression, endogenous oscillation, and noise, and this improves the model's ability to capture the physiological data. Based on the augmented inhibitory gating model, we make predictions regarding the model's response to pure tone stimuli, and evaluate these predictions by comparison with the

available physiological data for pure tones. Implications for general auditory computation are discussed.

An Inhibitory Gating Model

A simple network model, proposed to explain interval selective properties of midbrain neurons observed in *Pollimyrus* (Crawford, 1997), is illustrated in Fig. 2A. The selective midbrain neuron, (**S**), receives both excitatory input from the medulla (**M**) and inhibitory input through an interneuron (**I**). The properties of synaptic inputs in combination with the properties intrinsic to a given selective output neuron, determine the particular time interval that is optimal for the output neuron. An IPSP in the model selective neuron (**S**) gives rise to post-inhibitory rebound when it is of sufficient strength and duration (Fig. 2B).

With a single click as an auditory stimulus, the model yields an EPSP and an IPSP, but no action potentials. A succession of appropriately timed clicks, however, causes neuron **S** to generate action potentials because each EPSP coincides with the PIR from the previous auditory input. Thus, the neuron generates a large number of action potentials at the best ICI, and action potentials generated in this manner are phase locked to the stimulus click train. When the time between clicks is too short or too long the output decreases; if the ICI is sufficiently different, such that the EPSP and PIR no longer coincide, no action potentials are generated.

Synaptic Input

We begin with a model for the input to the selective cell. Both excitatory and inhibitory inputs are modeled as conductance changes in the selective neuron **S**, caused by presynaptic action potentials in **M** and **I** (Fig. 2A). The conductance changes are described using the following alpha equations (Rall, 1967).

$$g_E(t) = \begin{cases} \sum_p \bar{g}_E(t - t_p) \left(\frac{e}{\tau_E}\right) \exp\left(\frac{-(t-t_p)}{\tau_E}\right), & (t - t_p) > 0 \\ 0, & \text{otherwise} \end{cases} \quad (1A)$$

$$g_I(t) = \begin{cases} \sum_p \bar{g}_I(t - t_p - \Delta) \left(\frac{e}{\tau_I}\right) \exp\left(\frac{-(t-t_p-\Delta)}{\tau_I}\right), & (t - t_p - \Delta) > 0 \\ 0, & \text{otherwise} \end{cases} \quad (1B)$$

Equations (1A) and (B) describe time-varying synaptic conductances in the selective neuron **S** activated due to the arrival of presynaptic action potentials. The t_p represent the times of action potentials in **M**, and Δ is the total time delay between action potentials at the medullary neuron (**M**) and the inhibitory interneuron (**I**). The conductance terms \bar{g}_E and \bar{g}_I represent the maximal conductance changes produced by the excitatory and inhibitory inputs, and the times at which the input conductances reach their maximal values are determined by the time constants τ_E and τ_I .

The excitatory current $I_E = g_E(t)(V - V_E)$ gives rise to EPSPs and the inhibitory current $I_I = g_I(t)(V - V_I)$ gives rise to IPSPs. Here, $V_E = 0$ and $V_I = -80$ are the reversal potentials for excitation and inhibition, respectively. Thus, the conductance change due to input from **M** results in suprathreshold depolarization of **S**, and the conductance change due to input from **I** hyperpolarizes **S**. The relative timing of excitatory and inhibitory input (as determined by τ_E , Δ , and τ_I) plays a fundamental role in determining the tuning of the interval selective neuron.

PIR and Leak Currents

Post-inhibitory rebound (PIR) is a long-duration, low-threshold spike produced in response to inhibition, thus the PIR current is crucial to providing a temporally selective response in our model. Following Wang et al. (1991), we modeled the PIR current by analogy to the fast sodium current of Hodgkin-Huxley, $I_P = g_P s_\infty^3 h (V - V_P)$. The conductance, g_P determines the time course of rebound depolarization, and $V_P = 120$ is the reversal potential for PIR. This expression was originally proposed to model the T-type Ca^{++} current of relay cells of the cat *halamus* (Coulter et al., 1989; Wang et al., 1991). Because we lack voltage-clamp data for these cells, we use a simplification of the original model (Wang and Rinzel, 1993) that retains only two dynamic variables, membrane potential V and inactivation h , while preserving the basic behaviors of the original model.

The activation variable s has fast dynamics, and so is replaced by the steady state activation function $s_\infty(V) = 1/(1 + \exp(-(V - 70)/7.8))$. The dynamics of inactivation is described by Eq. (2):

$$\frac{dh}{dt} = \frac{\phi_h}{\tau_h(V)} [h_\infty(V) - h], \quad (2)$$

where $h_\infty(V) = 1/(1 + \exp((V - 84)/11))$, and the time constant for inactivation is also voltage dependent, $\tau_\infty(V) = h_\infty(V) \exp((V + 162.3)/17.8)$. The dimensionless parameter ϕ_h scales the time course of inactivation. The constants in these equations are the same as those reported by Wang and Rinzel (1993), with the exception that the half-activation points for $s_\infty(V)$, and $h_\infty(V)$ have been shifted slightly in the negative direction.

The leak current $I_L = g_L(V - V_L)$ represents the sum of all passive currents. The conductance g_L determines the passive time constant of the membrane, and the reversal potential V_L is responsible for setting the resting level of the neuron. When set within a certain range, however, V_L can qualitatively alter the steady-state behavior of the neuron, causing it to generate an endogenous subthreshold oscillation (cf. Wang et al., 1991), a possibility we explore below. Together, the PIR and leak currents determine the intrinsic time scale of the selective neuron (parameters g_L , ϕ_h , and g_L) affecting the width of the cell's interval selectivity function, and, to some extent, its peak.

Hodgkin-Huxley Currents

We also use a simplified model for action potential generation, because detailed patch-clamp data is not available for the *Pollimyrus* neurons. For this job we choose a dimensionality-reduced form of the Hodgkin-Huxley sodium (I_{Na}) and potassium (I_{K}) currents (Fitzhugh, 1961; Krinskii and Kokoz, 1973; Rinzel, 1985; Rose and Hindmarsh, 1989), with a persistent (non-inactivating) sodium current ($I_{\text{Na}(P)}$) (see Wang, 1994). The potassium current has the form $I_{\text{K}} = g_{\text{K}} n^4 (V - V_{\text{K}})$, where the inactivation variable n has the dynamics

$$\frac{dn}{dt} = \frac{\phi_n}{\tau_n(V)} [n_\infty(V) - n], \quad (3)$$

and $n_\infty = \alpha_n/(\alpha_n + \beta_n)$, $\alpha_n(\sigma_{\text{K}}, V) = -0.01(V + 45.7 - \sigma_{\text{K}})/(\exp(-0.1(V + 45.7 - \sigma_{\text{K}})) - 1)$, $\beta_n(\sigma_{\text{K}}, V) = 0.125 \exp(-(V + 55.7 - \sigma_{\text{K}})/80)$, $\tau_n = 1/(\alpha_n + \beta_n)$, $\phi_n = 200/7$, $g_{\text{K}} = 45 \text{ mS/cm}^2$, and $V_{\text{K}} = -80 \text{ mV}$.

The sodium current is $I_{\text{Na}} = g_{\text{Na}} m_\infty^3 (0.85 - n)(V - V_{\text{Na}})$, where inactivation, h , is replaced by $(0.85 - n)$ according to the empirical observation that during spike generation the kinetic variables h and n approximately satisfy the linear relationship $n + h = 0.85$ (FitzHugh, 1961). In addition, due to its fast time course, the dynamic variable m is replaced by its equilibrium

function $m_\infty = \alpha_m / (\alpha_m + \beta_m)$, where $\alpha_m(\sigma_{\text{Na}}, V) = -0.1(V + 29.7 - \sigma_{\text{Na}}) / (\exp(-0.1(V + 29.7 - \sigma_{\text{Na}})) - 1)$, $\beta_m(\sigma_{\text{Na}}, V) = 4 \exp(-(V + 54.7 - \sigma_{\text{Na}})/18)$, $g_{\text{Na}} = 63 \text{ mS/cm}^2$, and $V_K = +55 \text{ mV}$. The persistent sodium current, ($I_{\text{Na}(P)}$) is similar to (I_{Na}) but without inactivation, $I_{\text{Na}(P)} = g_{\text{Na}(P)} m_\infty^3 (V - V_{\text{Na}})$, and $g_{\text{Na}(P)} = 13.5 \text{ mS/cm}^2$. The parameters σ_K , σ_{Na} , and $\sigma_{\text{Na}(P)}$ are used to determine the action potential threshold of the model neuron.

Assembling the Model

Summarizing to this point, our model of interval selectivity contains seven currents, which can be grouped into three functional categories. First, presynaptic inputs are modeled using excitatory (I_E), and inhibitory (I_I) currents, whose time course primarily determines the tuning of the selective cell. Second, intrinsic properties of the selective neuron are captured as a post-inhibitory rebound (PIR) current (I_P) plus a leak current (I_L). The PIR current is responsible for the interval selective nature of the cell; together I_P and I_L determine the intrinsic time scale of the post-inhibitory rebound, which is the primary determinant of the width of the interval selectivity function. Third, action potential generation is captured using simplified Hodgkin-Huxley sodium (I_{Na}) and potassium (I_K) currents, plus a persistent sodium current ($I_{\text{Na}(P)}$). These currents generate action potentials, and have subtle effects on other aspects of cell behavior. Equation (4) combines these into a differential equation that relates the time derivative of membrane voltage to the seven membrane currents.

$$\begin{aligned} C_m \frac{dV}{dt} &= -I_E - I_I - I_P - I_L - I_{\text{Na}} - I_K - I_{\text{Na}(P)} \\ &= -g_E(t)(V - V_E) - g_I(t)(V - V_I) \\ &\quad - g_P s_\infty^3 h(V - V_P) - g_L(V - V_L) \\ &\quad - g_{\text{Na}} m_\infty^3 (.85 - n)(V - V_{\text{Na}}) \\ &\quad - g_K n^4 (V - V_K) - g_{\text{Na}(P)} m_\infty^3 (V - V_{\text{Na}}) \end{aligned} \quad (4)$$

Here, $C_m = 1 \mu\text{F/cm}^2$. To investigate whether this model adequately reproduced the observed physiology, model simulations were written in Matlab (5.3) and run on Sun Workstation (Solaris 4.4.1). The differential equations describing the behavior of the interval selective cell (Eqs. (2)–(4)) were solved numerically using Matlab's variable-order stiff solver (Matlab function *ode15s*) and some simulations were verified using a

modified Rosenbrock formula of order 2 (Matlab function *ode23s*; see Shapine and Reichelt, 1997).

Results for the Inhibitory Gating Model

Interval Selectivity

We first ran several simulations to investigate the ability of the model circuit to operate as a tuned temporal filter, responding to clicks presented at some inter-click intervals but not others. Input from the medulla was assumed to be time locked to the acoustic stimulus, and to consist of one action potential per click. Action potential times (t_p) were used to generate a time course of input conductances, both excitatory $g_E(t)$ and inhibitory $g_I(t)$, according to Eqs. (1A and B). The conductance changes drove the model and each simulation provided a trace of membrane potential in response to a click train. Nine stimulus ICIs were used (9, 10, 13, 18, 24, 33, 44, 59, and 80 ms; ICI's for which data was collected in the midbrain neurons) each click train had a duration of 100 ms.

To constrain the fits of the model output to data from *Pollimyrus* midbrain neurons, we identified physiologically plausible parameter ranges using measurements that were available for other neural systems from the literature, because the appropriate biophysical measurements have not yet been made in *Pollimyrus*. To test the tuning properties of the circuit, the parameters τ_E , τ_I , and Δ (Eq. (1A) and (B)) were then varied to manipulate the timing of EPSPs and IPSPs, and the parameters g_P , g_L , and ϕ , were varied to control the time course of post-inhibitory rebound. We fixed $V_L = 2 \text{ mV}$, $\bar{g}_E = .25 \text{ nS/cm}^2$, and $\bar{g}_I = .5 \text{ nS/cm}^2$.

Representative results of these simulations are illustrated in Fig. 3. Panel A (top) shows stimulation at several ICIs, with timing parameters $\tau_E = .75 \text{ ms}$, $\tau_I = 1.5 \text{ ms}$, and $\Delta = 2.25$ and rebound parameters $\phi_h = 6$, $g_P = 1.2 \text{ nS/cm}^2$, and $g_L = .6 \text{ nS/cm}^2$. A single stimulus ICI (10 ms) elicits a train of phase-locked action potentials; at shorter and longer ICIs membrane potential follows the stimulus (separate EPSPs, IPSPs, and PIRs are clearly visible at 24 ms), but no action potentials are generated. The model neuron is tuned to an ICI of 10 ms. Panel A (bottom) shows three selectivity functions that result from increasingly larger values of τ_E , τ_I , and Δ : best ICI is increased. Thus, other things being equal, these three parameters determine the best ICI of the model circuit. Panel B (top) shows membrane potential traces for a circuit tuned to 18 ms,

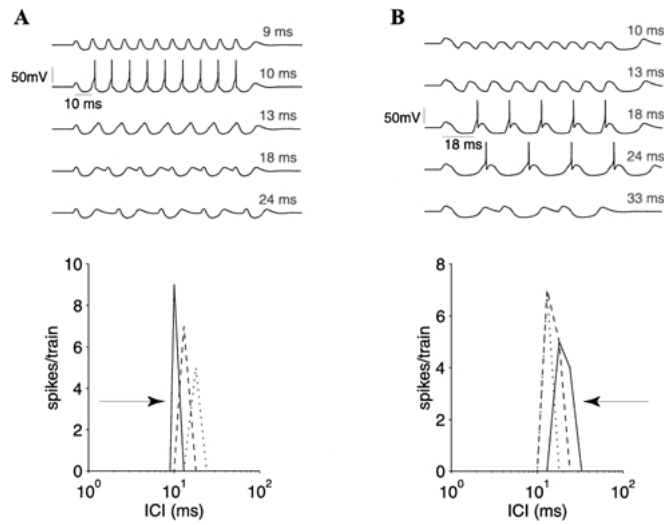


Figure 3. Interval selective responses modeled using the inhibitory gating hypothesis. **A:** Top. The response of a single model neuron (input timing: $\tau_E = .75$ ms, $\tau_I = 1.5$ ms, and $\Delta = 2.25$ and rebound timing: $\phi_h = 6$, $g_P = 1.2$ nS/cm², and $g_L = .6$ nS/cm²) to stimulation at five different ICIs. Best ICI is 10 ms. Bottom. An interval selectivity curve for the neuron above (solid line) shown with the responses of two other model neurons generated by varying input timing (dashed: $\tau_E = 1$ ms, $\tau_I = 2$ ms, and $\Delta = 3$ ms; dotted: $\tau_E = 2$ ms, $\tau_I = 4$ ms, and $\Delta = 6$ ms). Best ICIs are 13 and 18 ms respectively. **B:** Top. The response of a single model neuron to stimulation at five different ICIs (input timing: $\tau_E = 2$ ms, $\tau_I = 4$ ms, and $\Delta = 6$ ms; rebound timing: $\phi_h = 4.5$, $g_P = 0.9$ nS/cm², and $g_L = 0.45$ nS/cm²). The bandwidth of the neuron is wider than the neuron of Panel A due to a slower time course of PIR. Bottom. An interval selectivity curve for the neuron above (solid line) shown with the responses of two other model neurons generated by varying input as in Panel A. Interval tuning and bandwidth are adjustable independently, to some extent, using these two different sets of parameters.

with $\tau_E = 1$ ms, $\tau_I = 2$ ms, and $\Delta = 3$ ms, where the values of the rebound parameters have been increased to slow the intrinsic time course of the selective cell using parameter values $\phi_h = 4.5$, $g_P = .9$ nS/cm², and $g_L = .45$ nS/cm². The effect is to increase the bandwidth, and this manipulation is effective across a range of ICIs as illustrated by the additional selectivity functions (Panel B, below).

These simulations show that within a biophysically constrained parameter range the model behaves as a tuned temporal filter. Variations in the relative timing of excitatory and inhibitory input act to tune the response of individual circuits, determining best ICI. Finally, variation in the intrinsic properties of the selective neuron govern the time course of PIR, and primarily determine the width of the selectivity function.

Comparison with Raster Data

Figure 4 shows several raster plots recorded from a single interval selective midbrain neuron (Crawford, 1997). The physiology matches the above simulation in certain respects, but it also reveals departures from the model's predictions. In agreement with the model, the neuron is tuned (best ICI = 18 ms) with a moderate

bandwidth (compare with Fig. 3B). At best ICI it generates (at most) one action potential per click, and these are strongly phase-locked with the click train (pointer in Panel C). However, several other aspects of the observed physiology are not predicted by the above model.

First, action potentials are seen in response to the first click at every ICI (pointer in Panel A), and the overall rate of action potentials diminishes over the length of each click train. This neuron also produces strong responses at ICI's far from its best ICI (e.g., 80 ms). Second, at very long ICI's multiple action potentials follow the initial spike, and their timing approximately matches the best ICI of the neuron (18 ms, pointer in Panel H). Third, this neuron displays spontaneous activity, with action potentials recorded both before and after the click trains (pointers in Panel G).

An Augmented Model: Synaptic Depression, Endogenous Oscillation, and Noise

The above observations point to several ways in which the original model might be augmented to better fit the physiology. The first discrepancy is that responses are usually seen to the first click and diminish over the

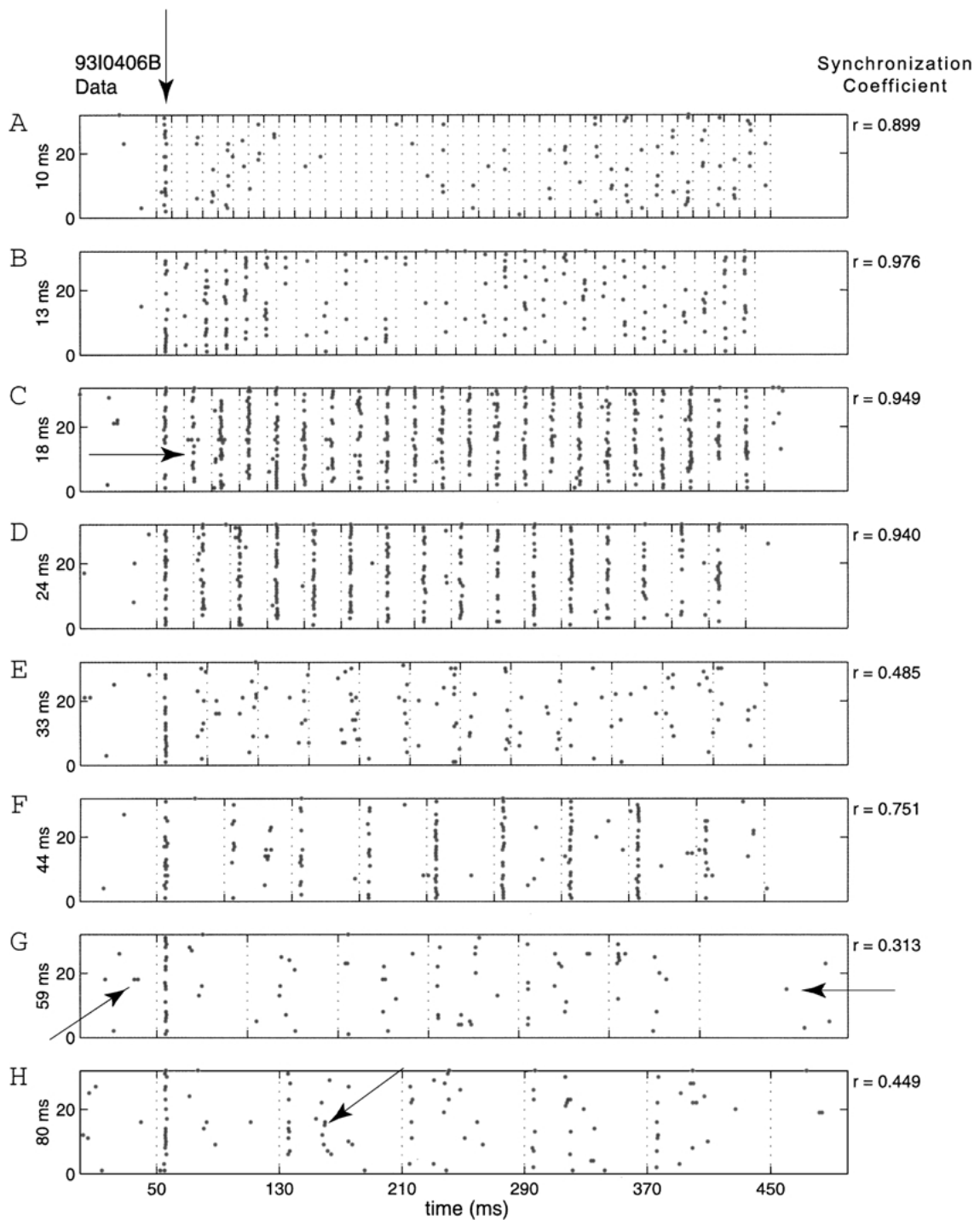


Figure 4. Full raster recordings for a single interval selective midbrain neuron. It is tuned for an inter-click interval of 18 ms and at best ICI it generates one action potential per click, strongly phase-locked with the click train (pointer in Panel C). Action potentials are seen in response to the first click at every ICI (pointer in Panel A), and the overall rate of action potentials diminishes over the length of each click train. Strong responses are seen at ICI's longer than best ICI (e.g., 80 ms): multiple action potentials follow the initial spike, and their timing approximately matches the best ICI of the neuron (pointer in Panel H). The neuron also displays spontaneous activity, with action potentials recorded both before and after the click trains (pointers in Panel G).

length of the click train. If a single stimulus click causes sufficient depolarization to generate an action potential, interval selective properties might arise from an interaction of factors: a decrease in synaptic efficacy, and a coincidence of EPSPs with rebound depolarization (inhibitory gating). This implicates a role for synaptic depression (Abbott et al., 1997; Varela et al., 1997; Chance et al., 1998). The involvement of synaptic depression also predicts that for very long ICIs, spikes would be generated in response to every click, and this prediction is supported by the rasters for 44, 59, and 80 ms click trains.

We included synaptic depression in the augmented model. The continuous time, fast synaptic depression model of Chance et al. (1998), was analytically solved to produce following difference equations for modifying the conductance terms \bar{g}_E and \bar{g}_I over the course of a click train. For excitatory synapses:

$$\begin{aligned}\bar{g}_{E(1)} &= \bar{g}_E \\ \bar{g}_{E(p+1)} &= 1 - (1 - d\bar{g}_{E(p)}) e^{-\Delta t/\tau}\end{aligned}\quad (5A)$$

and similarly, for inhibitory synapses:

$$\begin{aligned}\bar{g}_{I(1)} &= \bar{g}_I \\ \bar{g}_{I(p+1)} &= 1 - (1 - d_I\bar{g}_{I(p)}) e^{-\Delta t/\tau}\end{aligned}\quad (5B)$$

Here $\Delta t = t_{n+1} - t_n$, is the time between action potentials, which is equal to the fixed ICI of the click train for the deterministic model. However, the model is also general enough to allow different ICIs within the same click train (below we add temporal jitter). The parameters d_E and d_I are the depression factors for excitatory and inhibitory synapses, respectively. Due to the effect of inhibition on the magnitude of PIR, we allow different depression factors, but for simplicity these are always manipulated together, $d_I = d_E^2$. For the studies reported here the value of d_E varies between .85 and 1.0. The recovery rate (τ), was the same for both types of synapses, and varies between 100 and 300 ms.

Figure 5A shows the result of one run of the model with synaptic depression, where input strength was $g_E = 0.4$ nS/cm² and $g_I = 0.35$ nS/cm² and depression parameters were set to $d_E = 0.9$, $d_I = 0.81$, and $\tau = 300$ ms. A spike is produced in response to the first click of every train, spikes diminish over the length of the click train, and for slow click trains, an action potential is generated in response to every click. This model neuron displays selectivity for a 13 ms ICI (input timing: $\tau_E = 1$ ms, $\tau_I = 2$ ms, and $\Delta = 3$) and interval selectivity arises from an interaction of two physiological

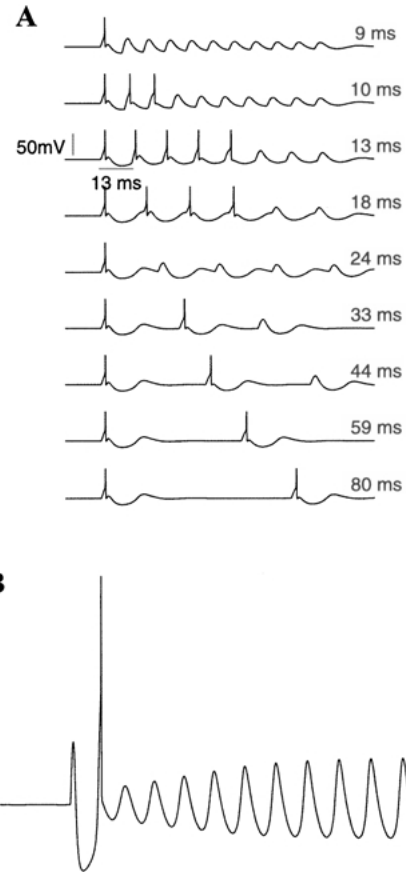


Figure 5. Behavior of the augmented model. **A:** Synaptic depression. Input strength parameters were chosen so that the neuron would generate an action potential for every click, $g_E = 0.4$ nS/cm² and $g_I = 0.35$ nS/cm², but with synaptic depression (Eqs. 5A and B) so that spikes diminished for non-preferred ICIs, $d_E = 0.9$, $d_I = 0.81$, and $\tau = 300$ ms. A spike is produced in response to the first click of every train, spikes diminish over the length of the click train, and for slow click trains, an action potential is generated in response to every click. This model neuron displays selectivity for a 13 ms ICI (input timing: $\tau_E = 1$ ms, $\tau_I = 2$ ms, and $\Delta = 3$; rebound timing: $\phi_h = 6$, $g_P = 1.2$ nS/cm², and $g_L = .6$ nS/cm²). **B:** Endogenous oscillation. Response to a single click. Parameters were chosen such that rebound depolarization would be strong enough to cause an action potential $g_E = 0.25$ nS/cm² and $g_I = 0.5$ nS/cm², and leak current reversal potential was set within a range that gives rise to endogenous oscillation $V_L = -77.5$.

mechanisms. A decrease in synaptic efficacy causes action potentials to cease after a time for non-preferred ICIs, but coincidence of EPSPs with PIR and preferred ICIs allows action potentials to continue for preferred ICIs (rebound timing: $\phi_h = 6$, $g_P = 1.2$ nS/cm², and $g_L = .6$ nS/cm²).

A second modification to the basic model is suggested by the additional spikes observed between clicks

in slow click trains. These provide evidence that post-inhibitory rebound alone can generate sufficient depolarization to cause action potentials in these neurons. Moreover, the fact that multiple rebound spikes can be seen at slow ICIs suggests an additional possibility: a spontaneous, subthreshold oscillation that entrains to stimulus clicks. This interpretation is consistent with known mechanisms of PIR (cf. Wang et al., 1991), and it could also contribute to an explanation of observed spontaneous activity.

The model described above is capable of generating such behavior with only a small change in parameter values. As leak current reversal potential (V_L) is lowered, the model neuron undergoes a Hopf bifurcation, and begins to generate an endogenous oscillation, consistent with the behavior described by Wang et al. (1991) for a similar PIR model. Figure 5B shows one simulation in which the V_L was lowered to a value of -77.5 mV (other parameters were set as in Fig. 3A). In this simulation, the neuron generates an initial rebound of sufficient amplitude to generate an action potential, and the following oscillation is in the subthreshold range. The model neuron generates endogenous oscillation for a range of values of V_L , with the value of the parameter determining the frequency and amplitude of the oscillation. If such behavior were present in the midbrain cells, this could explain the multiple rebound spikes observed in the raster plots.

Lastly, the variability of the selective responses requires a final modification to the basic model, the addition of two noise sources to model the variability observed in midbrain physiology. The first noise source is at the input. Action potentials in the medulla are known to be synchronized to acoustic input with temporal jitter, and observed synchronization coefficients fall primarily within the range $0.9 < r < 1$ (Suzuki et al., 2002). To model this property of midbrain input, gaussian noise (mean 0, variance Q_m) was used to jitter action potential times (t_p), where Q_m ranged from 0.25 to 1.0 ms². An additional stochastic component was added to Eq. (4) to model variability in the membrane potential of the interval selective cell itself. A gaussian noise current (mean 0, variance Q_V) captured variability in the simulated neuron, as in Eq. (4A).

$$C \frac{dV}{dt} = -I_E - I_I - I_P - I_L - I_{Na} - I_K - I_{Na(P)} - \sqrt{Q_V} \zeta(t) \quad (4A)$$

The noise current is instrumental in producing variability in rebound spike times, and, in conjunction with en-

dogenous subthreshold oscillations, can produce spontaneous activity in the model neurons, described next.

Results for the Augmented Model

Fits were generated to match the selectivity curves for nine midbrain neurons (Crawford, 1997) matching the observed physiology in detail, by examining the recorded raster plots and choosing parameters to mimic each cell's behavior, as described above. First, we illustrate this process by presenting a complete raster for one model neuron, shown above as Fig. 4. Next, we evaluate the fits to all nine cells by comparing interval selectivity curves of the model with those of the midbrain neurons. Finally, we verify the parameter values by comparing the pure tone responses of the midbrain neurons to those of the model. Parameter values were taken from the click train fits, so the simulations provided true predictions of pure tone responses, and thus a strong test of the model. As before, simulations were run by numerically solving the model Eqs. (2), (3) and (4A). For the following stochastic simulations, however, both Matlab ODE solvers were modified for simulation of stochastic differential equations (Hairer and Wanner, 1991).

A Complete Model Raster

The augmented model was used to generate fits for the rasters of Fig. 4; Fig. 6 shows the rasters generated by the model. The complete parameter set for this simulation is provided in column 3 of Table 1. The behavior of the augmented model matches this neuron's physiology in most respects. The model neuron is well tuned with a best ICI of 18 ms, and at its best ICI it generates an action potential for almost every click. Action potentials near the best ICI are also strongly phase-locked with the click train (pointer in Panel C). Moreover, action potentials are seen in response to the first click of the train at every ICI (pointer in Panel A), and the overall rate of action potentials diminishes over the duration of each click train. The model also produces strong responses at longer ICIs. For the slow click trains (e.g., 80 ms) multiple action potentials follow the initial spike due to PIR and endogenous oscillation, thus and their timing approximately matches the best ICI of the neuron (pointer in Panel H). Finally, the model displays spontaneous activity, with action potentials recorded both before (pointer in Panel D) and after (pointer in Panel G) the click trains. Spontaneous activity is due

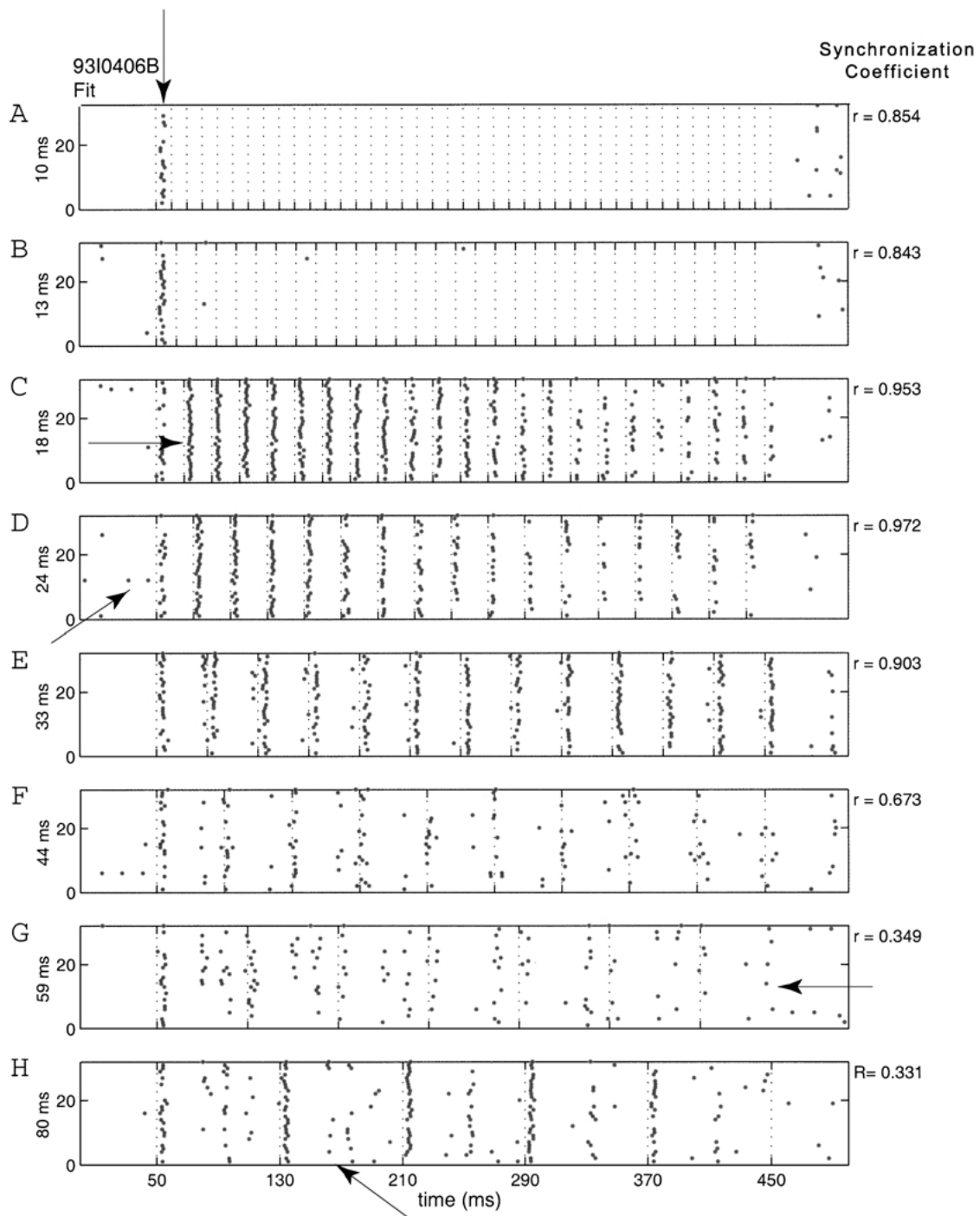


Figure 6. Full rasters for the augmented inhibitory gating model (compare with Fig. 4). The model neuron is well tuned with a best ICI of 18 ms, where it generates an action potential for almost every click, and action potentials near the best ICI are strongly phase-locked with the click train (pointer in Panel C). Action potentials are seen in response to the first click of the train at every ICI (pointer in Panel A), and the overall rate of action potentials diminishes over the duration of each click train. The model also produces strong responses at longer ICIs. For slow click trains multiple action potentials follow the initial spike due to PIR and endogenous oscillation, thus and their timing approximately matches the best ICI of the neuron (pointer in Panel H). Finally, the model displays spontaneous activity, with action potentials recorded both before (pointer in Panel D) and after (pointer in Panel G) the click trains.

Table 1. Parameters and constants, and the value ranges used in the model to generate fits to the physiological data.

Cell	302	308	406	407	602	502	504	603	605	Min	Max	Mean
<i>Input timing</i>												
τ_E ms	1.8	1.0	3.0	1.5	1.5	1.4	1.4	1.0	1.3	1.0	1.8	1.4
τ_I ms	3.6	1.0	6.0	1.5	1.5	1.4	1.4	1.0	1.3	1.0	3.6	1.7
Δ ms	5.4	3.0	4.5	4.5	4.5	4.2	4.2	3.0	3.9	3.0	5.4	4.1
<i>Rebound timing</i>												
ϕ_h	6.6	4.2	9.0	30.0	6.0	30.0	30.0	10.0	27.0	4.2	30.0	17.0
g_T mS/cm ²	1.320	0.840	1.800	6.000	1.200	6.000	6.000	2.004	5.400	0.840	6.000	3.396
g_L mS/cm ²	0.660	0.420	0.900	3.000	0.600	3.000	3.000	1.002	2.700	0.420	3.000	1.698
<i>Input strength</i>												
\bar{g}_E mS/cm ²	0.050	0.100	0.400	0.150	0.025	0.550	0.550	0.800	0.800	0.025	0.800	0.381
\bar{g}_I mS/cm ²	0.600	0.500	0.500	0.900	0.525	0.750	0.750	0.400	0.400	0.400	0.850	0.586
<i>AP threshold</i>												
σ_K mV	20.83	16.20	17.37	12.37	18.20	9.20	9.33	24.95	11.03	9.20	24.95	14.51
σ_{Na} mV	13.83	9.20	10.37	5.37	11.20	2.20	2.33	17.95	4.03	2.20	17.95	7.51
$\sigma_{Na(P)}$ mV	5.83	1.20	2.37	-2.63	3.20	-5.80	-5.68	9.95	-3.97	-5.80	9.95	-0.49
<i>Synaptic depression</i>												
d_E	0.95	0.94	0.95	0.97	0.85	0.99	0.99	0.99	0.99	0.85	0.99	0.96
d_I	0.90	0.88	0.90	0.94	0.72	0.98	0.98	0.98	0.98	0.72	0.98	0.92
τ ms	300	300	300	300	120	300	200	300	100	100	300	247
<i>Rebound type</i>												
V_L mV	-77.00	-77.00	-77.75	-76.25	-76.50	-76.50	-76.50	-76.25	-77.00	-77.75	-76.25	-76.75
<i>Noise</i>												
Q_m ms	1.0	1.0	1.0	1.0	1.0	0.5	0.5	0.5	0.5	0.5	1.0	0.8
Q_V mV	2.0	2.0	2.0	8.0	2.0	1.0	1.0	1.0	1.0	1.0	8.0	2.2

Conductances and time constants subscripted E describe events in S due to the M to S synapse (EPSP), and those with subscript I describe the events in S due to the I to S synapse (IPSP; see Fig. 2). The value ranges shown for input conductances (\bar{g}_E , \bar{g}_I) are the maximum values, and input time constants denote time required for the alpha equations to reach maximum conductance. The leak (L) and PIR (P) currents are endogenous to neuron S.

to an interaction between endogenous subthreshold oscillation and the membrane potential noise. Finally, the model matches the observed level of synchronization well, with modest synchronization at short ICIs, strong synchronization near best ICI, and weak synchronization at longer ICIs. The latter effect is due primarily to the generation of multiple action potentials in response to each click.

Fits: Click Train Data

We next fit selectivity curves for nine neurons from three different fish, to which stimuli were presented at 125 dB peak re: 1 μ Pa (Crawford, 1997). Thirty-two runs were simulated for each model neuron, and for each click train of a given inter-click-interval. Each

click train was 400 ms in duration, and in addition, 50 ms of prestimulus behavior and 50 ms of poststimulus behavior was simulated to match the raster recordings (as shown in Fig. 6). To fit the click train data, interval-selectivity curves were generated for direct comparison with the physiology. Input timing, input strengths (excitatory and inhibitory), rebound timing, rebound characteristics (gated versus oscillating), and synaptic depression parameters were chosen for each cell, using the techniques described above, to match the raster recordings as accurately as possible over the full range of stimulus ICIs. In addition, noise levels and thresholds were chosen to match individual physiology. To evaluate the parameter choices, two types of interval selectivity curves were calculated, total spikes per stimulus train (Fig. 7, left) and mean spikes per

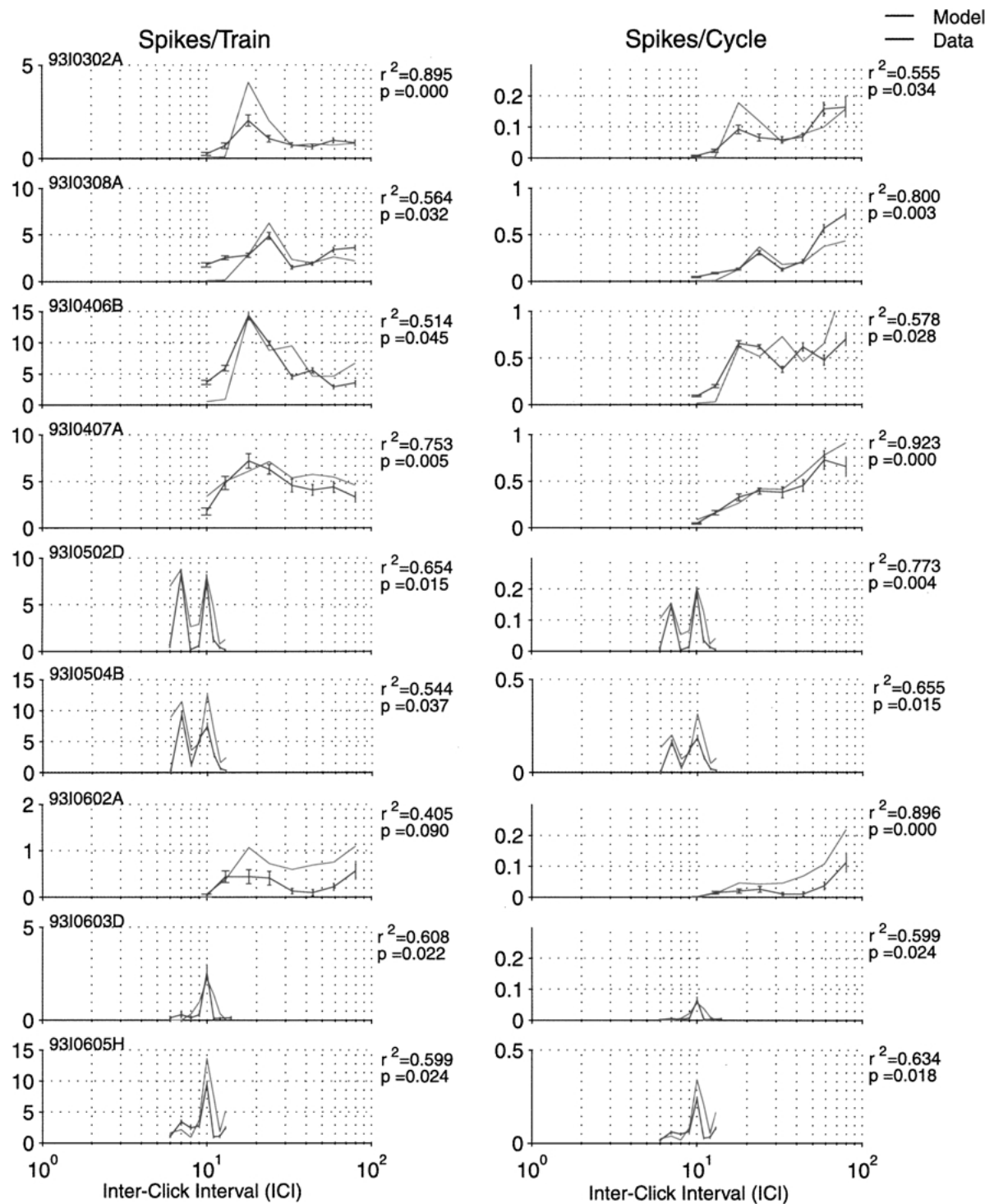


Figure 7. Interval selectivity curves measured both as spikes per train (left column) and spikes per click (right column) for nine cells (rows). Midbrain neuron data are shown in black (with error bars), model fits are shown in gray. Correlation coefficients and significance levels for the fits are shown to the right. Note that all neurons were initially tested in the 10–80 ms range, but several (neurons 5–6, and 8–9, from the top) gave little or no response except at the shortest intervals (10–13 ms). These neurons were re-tested in the shorter interval ranges shown (6–14 ms) where they produced robust responses. Model fits were restricted to these ranges.

stimulus click (Fig. 7, right). Parameters for each cell were manipulated until the both curves correlated significantly ($p < .05$) with the physiologically observed curves. Complete parameters for all nine fits are provided in Table 1.

Figure 7 compares the selectivity curves for the nine model neurons with the physiological data. Two features of this display are striking. The first is that interval selective midbrain neurons display quite varied physiology. Broadly speaking, cells are tuned either to shorter intervals (7–10 ms) or to longer intervals (13–24 ms). Some are quite sharply tuned, other selectivity functions are rather broad, and two interval-selective neurons displays double-peaked selectivity functions. The second striking feature is the quality of the model fits to this data. Correlation coefficients ranged from .405 to .895 for spikes per train, and from .555 to .923 for spikes per click. With one exception, both measures were highly correlated for all cells; in one case spikes per click curves were highly correlated, however, the very low overall number of spikes made a closer fit impossible in terms of spikes per train. Finally, detailed physiology matched the model's behavior well (not shown). The main discrepancy was that overall the model was more strongly synchronized to the click trains (mean $r = .893$) than the midbrain neurons (mean $r = .504$). Thus, the model interval selective neurons, generated through the mathematical implementation of an inhibitory gating mechanism, generated responses that were remarkably close to those observed in the auditory midbrain of *Pollimyrus*. Responses to click trains found excellent correspondence both in the temporal patterns of output spikes, and in the ICI-dependence of the responses.

Predictions: Pure Tone Responses

Our model was developed to provide insight into the mechanisms that underlie sensitivity to click train intervals, and the model worked well for this stimulus. To further evaluate the model, we examined responses to a different kind of stimulus, pure tones. In the physiological study, each neuron was stimulated with several pure tones (Crawford, 1997), and pure tones elicited distinctive, non-phase locked, responses in interval selective neurons. At least one complete raster response for a tone presented at 20–30 dB re: 1 μ Pa was available for seven of the nine interval selective neurons. Using the parameters that successfully simulated the response of individual neurons to click trains (Figs. 6 and 7), we

attempted to predict responses of these same neurons to tones of various frequencies. Thus, the model was used to obtain a true prediction of the response to a very different kind of stimulus, and this provided a strong test of the model. Initial runs indicated that the most important discrepancy between model predictions and midbrain responses to tones was that overall the model generated fewer action potentials. Surmising that the reason for this might be stronger input from the medulla for pure tones, we increase the input strength parameters by 25% for all model neurons and then re-ran the simulations. Other parameters were identical to those fit to click train data.

Many of the selective midbrain neurons responded to tones with a short burst of action potentials at tone onset. The model neuron predicted onset responses for several parameter sets. After the initial burst of action potentials caused by early excitation, the rapid succession of inputs causes the membrane potential to reach steady state well below the action potential threshold and no additional action potentials occurred during the stimulus (compare Fig. 8A and B). The neuron displayed greater spontaneous activity than did the model in the pure tone simulations, however, for these parameter values the model displayed spontaneous activity for the click train fits as well (shown in Fig. 6). In other cases model neurons predicted sustained responses to tones (Fig. 6C), and several of the selective biological neurons showed similar responses (Fig. 6D). In this case, the neuron also displays post-stimulus activity, which was most probably a neural response to ringing in the tank. Out of the seven cases tested, six matched the qualitative response of the biological neuron. The main difference, illustrated in Fig. 8, is that the model neurons generated fewer action potentials over all than the biological neurons did. Perhaps this is not too surprising, because the only difference between a pure tone and a click train in our model was the interval between action potentials arriving from the input neurons, **M** and **I**. It seems reasonable to assume that there may be other differences as well that are not accounted for in this simple model. Nevertheless, the quality of the model's predictions regarding pure tone responses was remarkably good.

Physiological Substrates for Inhibitory Gating in Pollimyrus

Evidence for the neural machinery required for the inhibitory gating mechanism comes from physiological

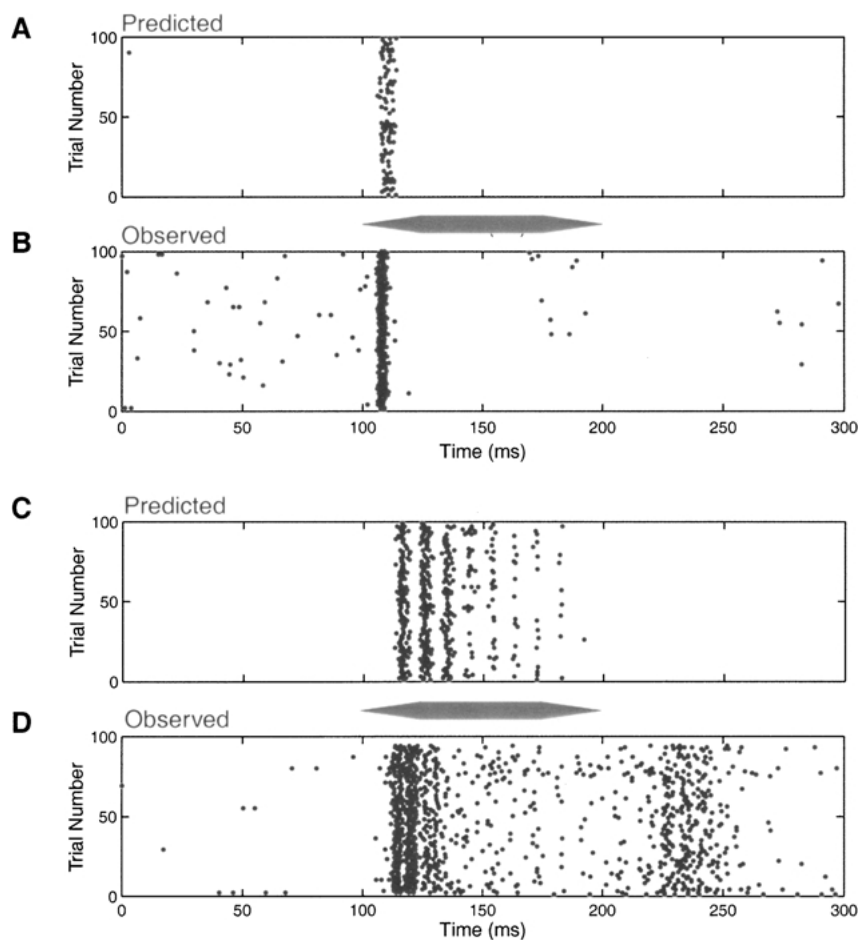


Figure 8. Predicted **A, C**: and observed **B, D**: responses to pure tone stimulation. Both onset and sustained responses were observed.

and anatomical studies of *Pollimyrus*. Neurophysiological experiments have demonstrated that highly synchronized spike trains are present in the midbrain (Crawford, 1993, 1997). These spike trains appear to be the input to the midbrain, provided by medullary projection neurons, and are ideally suited to providing the input required by the model. Additionally, recordings from midbrain neurons have provided evidence of both sound-induced inhibition and inhibitory rebound. The immunohistochemistry of the auditory midbrain also indicates that there are neurons containing the neurotransmitter γ -aminobutyric acid (GABA, Mugnaini and Maler, 1987). Neuroanatomical studies have revealed that a pair of lemniscal nuclei (IRN) form a feedback loop for the auditory midbrain, and this loop could provide the delayed inhibitory input needed for gating (Kozloski and Crawford, 1998b). These observations support the plausibility of this mechanism in

Pollimyrus. Additional biophysical studies of the auditory neurons will provide important new information for evaluation of the model.

Discussion

A key question for auditory temporal computation regards the source of neural delays sufficient to yield analysis on a time scale relevant for the analysis of communication sounds. The nervous system must analyze temporal events on a time scale of tens to hundreds of milliseconds in this context, and the axonal conduction delays that play a crucial role in binaural processing of microsecond time disparities (Carr, 1993), are not adequate for neural processing of these longer duration temporal cues. The delays produced through the post-inhibitory-rebound mechanisms, however, may represent a general solution for auditory temporal

computation in the range of a few to hundreds of milliseconds (Sullivan, 1982; Margoliash, 1983; Suga, 1988; Casseday et al., 1994; Buonomano and Merzenich, 1995; Crawford, 1997; Hooper, 1998).

Our results show that a simple network model, constrained by biophysical properties of real neurons, can predict the responses of interval-selective neurons in the auditory midbrain of a vertebrate animal. The underlying mechanism gains plausibility for *Pollimyrus* from neural circuitry appropriate for the proposed network, existence of the required synchronized input to the midbrain, evidence for GABA-mediated inhibition, and inhibitory rebound. The model closely fits the observed interval-selectivity curves for naturalistic click-train stimuli reported previously (Crawford, 1997). It also produced output resembling the complex physiological responses of interval selective cells to pure tones. Thus, this model represents a realistic proposal for auditory temporal computation in the analysis of communication sounds, whether the simple sounds of fish courtship or the complex sounds of human speech.

One important benefit of this theoretical formulation is that it provides clear predictions for further neurophysiological evaluation of the inhibitory gating hypothesis in *Pollimyrus*. The output of the model depends specifically on the precise timing of the inputs, and not simply the average rate of input. Thus the model predicts that irregular click trains would produce little output even if the average interval of the input were appropriate. Physiological output should decline as irregularity, or jitter, in the stimulus click trains is increased. Click-train-like stimuli can also be created from tone complexes added in zero starting phase. Randomizing the starting phases in this kind of stimulus is expected to introduce jitter to the timing of the input action potentials and thus reduce physiological output in a similar fashion. This is an important experiment because the manipulation does not change the amplitude spectrum of the stimulus. There are also clear predictions from the model regarding membrane potential excursions during stimulation (Fig. 2), and these can be evaluated in future intracellular studies. The kinetics of the currents underlying EPSPs, IPSPs, and PIR can be measured. The suspected inhibitory input to selective neurons can be blocked pharmacological agents (Fuzessery and Hall, 1996; Casseday et al., 2000), and this should eliminate interval-selectivity in *Pollimyrus*.

Data from other species support the proposed temporal mechanism as well. Frogs and toads (*Anurans*) make amplitude modulated mating calls, many of which are

similar to the grunts of *Pollimyrus* and other fishes (Fine et al., 1997; Gerhardt, 1994; Myberg, 1997). Midbrain auditory neurons in some of these animals are known to be selective (*tuned*) to the AM rates used in sound production (Feng et al., 1990; Alder and Rose, 1998). These neurons are physiologically similar to the selective neurons in *Pollimyrus* in that they have similar narrow ranges of preferred intervals that elicit maximal spike output. The two types of neurons have best repetition rates in the 40–100 pulses per second range. In contrast to *Pollimyrus*, the selective neurons in frogs (*Rana pipiens*) require a minimum number (median ≈ 8) of consecutive correct intervals before they begin to spike, and are thought to depend upon an *integration process* (Alder and Rose, 1998). Thus, these *pulse-integration* (PI) neurons appear to reflect both (1) a physiological mechanism for interval selectivity and (2) a mechanism for counting the number of times the temporal criterion has been reached. It is not yet known which mechanism underlies the interval selectivity of PI neurons, but an inhibitory gating mechanism is a clear possibility. The inhibitory gating hypothesis is consistent with the finding that application of GABA antagonists can eliminate interval selectivity in frog midbrain neurons (Hall, 1994). The selectivity recorded in PI neurons may be produced by circuits that provide input to the PI neurons, and the PI neurons may then integrate a succession of inputs to produce the observed dependence on stimulus pulse number. This integration process could explain why the PI responses lack the synchronization and relatively short latencies that are characteristic of selective neurons in *Pollimyrus*.

It has also been hypothesized that selectivity for sound duration in mammals could be created through a mechanism involving a combination of excitatory and inhibitory inputs to a duration tuned neuron, with inhibitory rebound gating the throughput of the excitatory input (Casseday et al., 1994; Fig. 1, Casseday et al., 2000). The transient excitatory input is delayed, and the inhibitory input is initiated at stimulus onset and sustained. If the duration of the sound is appropriate, inhibitory rebound following sound offset will coincide with the excitatory input and produce a facilitated response. Thus, duration tuning is determined by the delay of the onset-elicited excitatory input (fixed), and by the timing of inhibitory rebound, determined by sound duration and locked to sound offset (variable). Though similar in some respects to the model we have developed for interval selectivity, there are important

differences. Most importantly, the duration mechanism will not yield selectivity to the intervals of click trains. Similarly, continuous sounds can overwhelm our inter-selectivity mechanism with inhibition and no selectivity for duration will be seen. This mechanism for duration tuning has received experimental support from whole cell recordings in the midbrain of bats and from pharmacology (Casseday et al., 1994), but more recent analysis of this system suggests that the original model is possibly overly simplistic and that multiple mechanisms may be involved (Casseday et al., 2000).

The models discussed to this point are based on properties of simple networks. Nevertheless, intrinsic membrane properties of single neurons, and properties of single synapses, might also contribute to periodicity selectivity. For example, sensitivity to very low frequency AM (5–10 Hz) in the electrosensory system of fish may be produced by through a combination of synaptic facilitation (high rate pass) and synaptic depression (low rate pass; Fortune and Rose, 2000). Although these mechanisms could contribute to the selective auditory neurons described here, they are not consistent with the short latency synchronized responses seen in *Pollimyrus* nor the influence of GABA blockade reported in frogs.

Comparison with other Computational Models

Other investigators have also undertaken modeling of auditory temporal analysis. Buonomano and Merzenich (1995) used slow inhibition and paired pulse facilitation in a model of cortical computation. Their neural circuits were generated randomly, and parameter values were fixed within neurons of a given type. An array of circuits was generated, each defined by its unique time-interval selectivity. However, their circuits did not produce the temporally structured responses we observed in our interval-selective auditory neurons, and they did not fit their model output to any other physiological data.

Hooper (1998) proposed a network model that incorporated both inhibition and post-inhibitory rebound. The model was based on the physiology of the crustacean pyloric motor system. In his neurons, the time it took for PIR to occur shifted as a function of the temporal properties of the input (e.g. ICI), and this shifting delay required that the output of multiple neurons be compared to arrive at any single duration. Extrapolating to processing in a hypothetical sensory system, Hooper suggests that a system of synaptic delays, in

combination with the physiology of individual neurons, could yield a perceptual system for the identification of specific temporal intervals (comparable to ICI) and event durations (comparable to click duration). However, the performance of this model has not yet been compared with data from temporally-sensitive sensory neurons. In *Pollimyrus*, interval selective neurons do not respond to different ICI's by shifting their firing time relative to clicks, and duration sensitive neurons have not yet been found. Thus, our model is relatively simple, using biophysical variables within realistic ranges, and captures the observed physiological responses of temporally-sensitive auditory neurons.

Human psychophysical studies have demonstrated similarities between time discrimination performance and motor pattern production (e.g., Ivry and Hazeltine, 1995). Many researchers have taken such evidence to indicate that discrimination and production of time intervals may share a common timing mechanism, perhaps in the cerebellum or basal ganglia. However, more recent studies suggest that perceptual and motor mechanisms may be quite independent. It has recently been demonstrated, for example, that sensorimotor synchronization is sensitive to subliminal timing changes, such that synchronization responses may not even be under voluntary control (Repp, 2000–2002). Moreover, sensitivity to temporal intervals has now been described in the midbrain sensory nuclei of a diversity of vertebrate species, including fishes, frogs, birds and mammals (Carr, 1993). Thus, in this comparative context, it seems unlikely that the temporal mechanisms for vertebrate perception are predominantly the domain of the cerebellum and basal ganglia. The type of mechanism modeled here could account for temporal discriminations, as required for the perception of prosody in language and rhythm in music, whether carried out in the midbrain (inferior colliculus) or in other brain regions. Thus, this study adds to a growing body of evidence that the perception and production of timing may arise from different neural systems.

Conclusion

Understanding how the nervous system processes temporal information is of broad relevance in understanding human and animal behavior. In auditory perception, extraction of the temporal features of acoustic signals is of particular importance. The dynamic model presented here, constrained by physiologically realistic parameters, yielded output that closely matched

observed physiological responses to temporal patterns in naturalistic sounds. The correspondence was close in the number of action potentials elicited, in the distribution of action potential times, and in action potential synchronization. The biophysical parameters we varied to reproduce the observed physiology could vary within the interval-selective circuits in the CNS. This and other predictions will be evaluated in future empirical work.

Acknowledgments

Research supported by NIH R01 DC01252 to JDC, and an NIH (NRSA) Post-doctoral Fellowship Award 1 F32 DC00347 to EWL. The authors are indebted to Viktor Jirsa, Farzan Nadim, Betty Tuller, Lindsay B. Fletcher and Aae Suzuki for valuable discussions, and critical comments on an earlier version of this manuscript.

References

- Abbott LF, Sen K, Varela JA, Nelson SB (1997) Synaptic depression and cortical gain control. *Science* 275: 220–224.
- Alder TB, Rose GJ (1998) Long-term temporal integration in the anuran auditory system. *Nature Neurosci.* 1: 519–523.
- Alder TB, Rose GJ (2000) Integration and recovery processes contribute to the temporal selectivity of neurons in the midbrain of the northern leopard frog, *Rana pipiens*. *J. Comp. Physiol. A* 186: 923–937.
- Bodnar DA, Bass AH (1999) Midbrain combinatorial code for temporal and spectral information in concurrent acoustic signals. *J. Neurophysiol.* 81: 552–563.
- Bregman AS (1990) *Auditory Scene Analysis: The Perceptual Organization of Sound*. MIT Press, MA.
- Buonomano DV, Merzenich MM (1995) Temporal information transformed into a spatial code by a neural network with realistic properties. *Science* 267: 1028–1030.
- Carr CE (1993) Processing of temporal information in the brain. *Ann. Rev. Neurosci.* 16: 223–242.
- Casseday JH, Ehrlich D, Covey E (1994) Neural tuning for sound duration: Role of inhibitory mechanisms in the inferior colliculus. *Science* 264: 847–850.
- Casseday JH, Ehrlich D, Covey E (2000) Neural measurement of sound duration: Control by excitatory-inhibitory interactions in the inferior colliculus. *J. Neurophysiol.* 84: 1475–1487.
- Chance FS, Nelson SB, Abbott LF (1998) Synaptic depression and the temporal response characteristics of V1 cells. *J. Neurosci.* 18: 4785–4799.
- Coulter DA, Huguenard JR, Prince DA (1989) Calcium currents in rat thalamocortical relay neurones: Kinetic properties of the transient, low-threshold current. *J. Physiol.* 414: 587–604.
- Crawford JD (1993) Central auditory neurophysiology of a sound-producing mormyrid fish: The mesencephalon of *Pollimyrus isidori*. *J. Comp. Physiol. A* 172: 1–14.
- Crawford JD (1997) Feature detection by auditory neurons in the brain of a sound-producing fish. *J. Comp. Physiol. A* 180: 439–450.
- Crawford JD, Cook AP, Heberlein AS (1997) Bioacoustic behavior of African fishes (Mormyridae): Potential cues for species and individual recognition in *Pollimyrus*. *J. Acoust. Soc. Am.* 102: 1200–1212.
- Crawford JD, Huang X (1999) Communication signals and sound production mechanisms of mormyrid electric fish. *J. Exp. Biol.* 202: 1417–1426.
- Cudmore RH, Large EW, Crawford JD (1998) Auditory temporal computation: A simple network model for feature extraction from communication sounds. Society for Neuroscience Annual Meeting (#77.6).
- Diekamp B, Gerhardt HC (1995) Selective phonotaxis to advertisement calls in the gray treefrog *Hyla versicolor*: Behavioral experiments and neurophysiological correlates. *J. Comp. Physiol. A* 177: 173–190.
- Edwards DH (1983) Feed-forward lateral inhibition and the DCMD neuron. In *IEEE Int. Conf. Sys, Man Cybern.* pp. 261–265.
- Fay RR (1978) Phase-locking in goldfish saccular nerve fibres accounts for frequency discrimination capacities. *Nature* 275: 320–322.
- Fay RR (1995) Perception of spectrally and temporally complex sounds by the goldfish (*Carassius auratus*). *Hearing Res.* 89: 146–154.
- Fay RR, Coombs S (1983) Neural mechanisms in sound detection and temporal summation. *Hearing Res.* 10: 69–92.
- Feng AS, Hall JC, Gooler DM (1990) Neural basis of sound pattern recognition in anurans. *Prog. Neurobiol.* 34: 313–329.
- Fine ML, Winn HE, Olla BL (1977) Communication in fishes. In: TA Sebeok, ed. *How Animals Communicate*. Indiana University Press, Bloomington, IN. pp. 472–517.
- Fizthugh R (1961) Impulses and physiological states in theoretical models of nerve membrane. *Biophys. J.* 1: 445–466.
- Fletcher LB, Crawford JD (2001) Acoustic detection by sound-producing fishes (Mormyridae): The role of gas-filled tympanic bladders. *J. Exp. Biol.* 204: 175–183.
- Fortune ES, Rose GJ (2000) Short-term synaptic plasticity contributes to the temporal filtering of electrosensory information. *J. Neurosci.* 20: 7122–7130.
- Furukawa T, Ishii Y (1967) Neurophysiological studies on hearing in goldfish. *J. Neurophys.* 30: 1377–1403.
- Fuzessery ZM, Hall JC (1996) Role of GABA in shaping frequency tuning and creating FM sweep selectivity in the inferior colliculus. *J. Neurophysiol.* 76: 1059–1073.
- Gerhardt HC (1994) The evolution of vocalizations in frogs and toads. *Ann. Rev. Ecol. Syst.* 25: 293–324.
- Hairer E, Wanner G (1991) *Solving Ordinary Differential Equations II, Stiff and Differential-Algebraic Problems*. Springer-Verlag, Berlin.
- Hall JC (1994) Central processing of communication sounds in the anuran auditory system. *Am. Zool.* 34: 670–684.
- Hooper SL (1998) Transduction of temporal patterns by single neurons. *Nature Neurosci.* 1: 720–726.
- Hoy RR, Pollack GS, Moiseff A (1982) Species recognition in the field cricket, *Teleogryllus oceanicus*: Behavioral and neural mechanisms. *Am. Zool.* 22: 597–607.
- Huber F, Thorson J (1985) Cricket auditory communication. *Sci. Am.* 253: 60–68.

- Ivry RB, Hazeltine RE (1985) Perception and production of temporal intervals across a range of durations: Evidence for a common timing mechanism. *J. Exp. Psych.: Human Percept. Perform.* 21: 3–18.
- Jenssen TA (1970) Female responses to filmed displays of *Anolis nebulosus* (Sauria, Iguanidae). *Anim. Behav.* 18: 640–647.
- Kozloski J, Crawford JD (1997) Emergence of temporal fidelity in the ascending auditory system of sound-generating fish. Abstract, Midwinter Meeting, Association for Research in Otolaryngology.
- Kozloski J, Crawford JD (1998a) Rate coding of sound features in second and third order auditory nuclei is computed from temporally structured first order spike trains. Society for Neuroscience Abstracts (#77.5).
- Kozloski J, Crawford JD (1998b) Functional neuroanatomy of auditory pathways in the sound-producing fish *Pollimyrus*. *J. Comp. Neurol.* 401: 227–252.
- Krinskii VI, Kokoz YM (1973) Analysis of equations of excitable membranes—I. reduction of the Hodgkin-Huxley equations to a second order system. *Biofizika* 18: 533–539.
- Langner G (1992) Periodicity coding in the auditory system. *Hearing Res.* 60: 115–142.
- Langner G, Schreiner CE (1988) Periodicity Coding in the inferior colliculus of the cat. I. Neuronal mechanisms. *J. Neurophys.* 60: 1799–1822.
- Large EW, Jones MR (1999) The dynamics of attending: How we track time varying events. *Psych. Review* 106: 119–159.
- Lee SH, Blake R (1999) Visual form created solely from temporal structure. *Science* 284: 1165–1168.
- Lloyd JE (1975) Aggressive mimicry in *Photuris* fireflies: Signal repertoires by *femmes fatales*. *Science* 197: 452–453.
- Lu Z, Fay RR (1996) Two-tone interaction in primary afferents and midbrain neurons of the goldfish, *Carassius auratus*. *Audit. Neurosci.* 2: 257–273.
- Margoliash D (1983) Acoustic parameters underlying the responses of song-specific neurons in the white-crowned sparrow. *J. Neurosci.* 3: 1039–1057.
- Marvit P, Crawford JD (2000) Auditory discrimination in a sound-producing electric fish (*Pollimyrus*): Tone frequency and click-rate difference detection. *J. Acoust. Soc. Am.* 108: 1819–1825.
- Moeng R, Popper AN (1984) Auditory responses of saccular neurons of the catfish, *Ictalurus punctatus*. *J. Comp. Physiol. A* 155: 615–624.
- Mugnaini E, Maler L (1987) Cytology and immunocytochemistry of the nucleus extrolateralis anterior of the mormyrid brain: Possible role of GABAergic synapses in temporal analysis. *Anat. & Embryol.* 176: 313–336.
- Myrberg, AA, Jr (1997) Underwater sound: Expanding relevance to behavioral functions among fishes and marine animals. *Mar. & Freshwater Behav. & Physiol.* 29: 3–22.
- Penna M, Lin WY, Feng AS (1997) Temporal selectivity for complex signals by single neurons in the torus semicircularis of *Pleurodema thaul* (Amphibia: Leptodactylidae). *J. Comp. Physiol. A* 180: 313–328.
- Plassmann W (1985) Coding of amplitude-modulated tones in the central auditory system of catfish. *Hearing Res.* 17: 209–217.
- Popper AN, Coombs S (1982) The morphology and evolution of the ear in actinopterygian fishes. *Amer. Zool.* 22: 311–328.
- Popper AN, Fay RR (1997) Evolution of the ear and hearing: Issues and questions. *Brain, Behav. Evol.* 50: 213–221.
- Rall W (1967) Distinguishing theoretical synaptic potentials computed for different somadendritic distributions of synaptic input. *J. Neurophys.* 30: 1138–1168.
- Repp BH (2000) Compensation for subliminal timing perturbations in perceptual-motor synchronization. *Psych. Res.* 63: 106–128.
- Repp BH (2001) Phase correction, phase resetting, and phase shifts after subliminal timing perturbations in sensorimotor synchronization. *J. Exp. Psych.: Human Percept. Perform.* 27: 600–621.
- Repp BH (2002) Automaticity and voluntary control of phase correction following event onset shifts in sensorimotor synchronization. *J. Exp. Psych.: Human Percept. Perform.* 28: 410–430.
- Rinzel J (1985) Excitation dynamics: Insights from simplified membrane models. *Fedn Proc.* 15: 2944–2946.
- Rose GJ, Capranica RR (1985) Sensitivity to amplitude modulated sounds in the anuran auditory nervous system. *J. Neurophys.* 53: 446–465.
- Rose RM, Hindmarsh JL (1989) The assembly of ionic currents in a thalamic neuron (Parts I–III). *Proc. R. Soc. Lond. B* 237: 267–334.
- Salmon M, Atsides SP (1968) Visual and acoustical signaling during courtship by fiddler crabs (genus *Uca*). *Am. Zool.* 8: 623–639.
- Schellart NAM, Popper AN (1992) Functional aspects of the evolution of the auditory system of actinopterygian fish. In: DB Webster, RR Fay, AN Popper, eds. *The Evolutionary Biology of Hearing*. Springer-Verlag, New York. pp. 295–322.
- Shampine LF, Reichelt MW (1997) The MATLAB ODE suite. *SIAM Journal of Scientific Computing* 18: 220–227.
- Suga N (1988) Auditory neuroethology and speech processing: Complex sound processing by combination-sensitive neurons. In GM Edelman, WE Gall, WM Cowan, eds. *Functions of the Auditory System*. Wiley, New York. pp. 679–720.
- Sullivan WE (1982) Possible neural mechanisms of target distance encoding in auditory system of the echolocating bat *Myotis lucifugus*. *J. Neurophysiol.* 48: 1033–1047.
- Suzuki A, Crawford JD (2000) The primary auditory input to the brain of sound-producing mormyrid fishes. Abstract, Midwinter Meeting, Association for Research in Otolaryngology.
- Suzuki A, Kozloski J, Crawford JD (2002) Temporal encoding for auditory computation: Physiology of primary afferent neurons in sound-producing fish. *J. Neurosci.* 22: in press.
- Varela JA, Sen K, Gibson J, Fost J, Abbott LF, Nelson SB (1997). A quantitative description of short-term plasticity at excitatory synapses in layer 2/3 of rat primary visual cortex. *J. Neurosci.* 17: 7926–7940.
- Wang XJ (1994) Multiple dynamical modes of thalamic relay neurons: Rhythmic bursting and intermittent phase-locking. *Neurosci.* 59: 21–31.
- Wang XJ, Rinzel J, Rogawski MA (1991) A model of the T-type calcium current and the low-threshold spike in thalamic neurons. *J. Neurophys.* 66: 839–850.
- Wang XJ, Rinzel J (1993) Spindle rhythmicity in the reticularis thalami nucleus: Synchronization among mutually inhibitory neurons. *Neurosci.* 53: 899–904.